NASA TECHNICAL MEMORANDUM

NASA TM X-2056

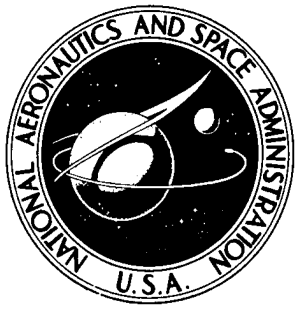


NASA TM X-2056

# DRAG CHARACTERISTICS OBTAINED FROM SEVERAL CONFIGURATIONS OF THE MODIFIED X-15-2 AIRPLANE UP TO MACH 6.7

*by Lawrence C. Montoya*

*Flight Research Center*
*Edwards, Calif. 93523*

NATIONAL AERONAUTICS AND SPACE ADMINISTRATION • WASHINGTON, D. C. • AUGUST 1970

| 1. Report No. | 2. Government Accession No. | 3. Recipient's Catalog No. |
|---|---|---|
| NASA TM X-2056 | | |

| 4. Title and Subtitle | 5. Report Date |
|---|---|
| DRAG CHARACTERISTICS OBTAINED FROM SEVERAL CONFIGURATIONS OF THE MODIFIED X-15-2 AIRPLANE UP TO MACH 6.7 | August 1970 |
| | 6. Performing Organization Code |

| 7. Author(s) | 8. Performing Organization Report No. |
|---|---|
| Lawrence C. Montoya | H-598 |
| | 10. Work Unit No. |
| 9. Performing Organization Name and Address | 722-51-00-01-24 |
| NASA Flight Research Center<br>P. O. Box 273<br>Edwards, California 93523 | 11. Contract or Grant No. |
| | 13. Type of Report and Period Covered |
| 12. Sponsoring Agency Name and Address | Technical Memorandum |
| National Aeronautics and Space Administration<br>Washington, D. C. 20546 | 14. Sponsoring Agency Code |

15. Supplementary Notes

16. Abstract

Flight tests were made with and without the lower ventral fin, dummy ramjet (including the modified fixed ventral fin), and ablative coating over the entire wetted area. Data were obtained at Mach numbers from 0.5 to 6.7 and free-stream Reynolds numbers from approximately $1.7 \times 10^8$ to $3.6 \times 10^7$ based on fuselage length. Angle of attack ranged from 0° to 11°, dynamic pressure from about 300 lb/ft$^2$ (14,364 N/m$^2$) to 770 lb/ft$^2$ (36,868 N/m$^2$), and altitude from approximately 3000 ft (914 m) to 102,000 ft (31,090 m).

Supersonic flight results showed an increase in drag coefficient caused by the ablative coating of 0.008 at a lift coefficient of 0 and 0.022 at a lift coefficient of 0.3. At subsonic speeds the average increase in drag coefficient was about 0.013 for lift coefficients of 0.3 and 0.4. The flight incremental increase in drag coefficient due to the ablative coating showed good agreement with compressible predicted values at low lift coefficients.

The average incremental increase in drag coefficient caused by the lower ventral fin and dummy ramjet was about 0.010 at subsonic speeds at a lift coefficient of about 0.3. The flight incremental increase in drag coefficient of the lower ventral fin between Mach 3.8 and 4.9 was about 0.006 at a lift coefficient of 0.1 and 0.014 at a lift coefficient of 0.3.

| 17. Key Words (Suggested by Author(s)) | 18. Distribution Statement |
|---|---|
| X-15 airplane - Drag increment - Ablative drag | Unclassified - Unlimited |

| 19. Security Classif. (of this report) | 20. Security Classif. (of this page) | 21. No. of Pages | 22. Price* |
|---|---|---|---|
| Unclassified | Unclassified | 28 | $3.00 |

*For sale by the Clearinghouse for Federal Scientific and Technical Information
Springfield, Virginia 22151

# DRAG CHARACTERISTICS OBTAINED FROM SEVERAL CONFIGURATIONS OF THE MODIFIED X-15-2 AIRPLANE UP TO MACH 6.7

Lawrence C. Montoya
Flight Research Center

## INTRODUCTION

Drag characteristics of the basic X-15 airplane were measured over a Mach number range extending from landing velocities to Mach 6 (refs. 1 and 2). After the basic X-15 program was completed, the number two X-15 airplane (X-15-2) was modified to expand its flight envelope and thus provide a testbed for a proposed ramjet test program (ref. 3). These modifications resulted in changes in the airframe which could affect the overall drag.

For several X-15-2 flights an ablative coating was applied to the surfaces of the airplane. Flights of the modified X-15-2 airplane were also made with a dummy ramjet installed on the modified fixed portion of the lower ventral fin.

The data for this paper were obtained during the X-15-2 envelope extension program in which the airplane was flown with and without the ablative coating, with and without the lower ventral fin, with combinations of these two configurations, and with the dummy ramjet. The changes in drag characteristics for these various configurations are documented in this paper, and the existing drag data are extended to higher Mach numbers. Flight results are presented for Mach numbers from 0.5 to 6.7 (the highest speed thus far obtained by a winged aircraft). All flight data are for power-off (glide), trimmed flight. Data from the present tests are compared with full-scale flight data from reference 2, unpublished wind-tunnel and flight data, and predictions.

## SYMBOLS

| | |
|---|---|
| $A$ | area, $ft^2$ ($m^2$) |
| $a_l$ | measured longitudinal acceleration (along aircraft reference axis), g units |
| $a_n$ | measured normal acceleration, g units |
| $C_D$ | drag coefficient, $\frac{D}{qS}$ |
| $C_{D_c}$ | forebody drag coefficient of a circular cylinder based on frontal area, $\frac{D}{q\ell d}$ |

| | |
|---|---|
| $C_f$ | average skin-friction coefficient for turbulent flow |
| $C_L$ | lift coefficient, $\frac{L}{qS}$ |
| $C_{p_b}$ | base pressure coefficient, $\frac{p_b - p}{q}$ |
| D | drag force along flight path, lb (N) |
| d | diameter or thickness, ft (m) |
| g | gravitational acceleration, ft/sec$^2$ (m/sec$^2$) |
| k | roughness height (protuberance), in. (m) |
| L | lift force normal to the flight path, lb (N) |
| L/D | lift-to-drag ratio |
| $l$ | length, ft (m) |
| M | free-stream Mach number |
| p | free-stream static pressure, lb/ft$^2$ (N/m$^2$) |
| $p_b$ | base static pressure, lb/ft$^2$ (N/m$^2$) |
| q | free-stream dynamic pressure, 0.7 $M^2p$, lb/ft$^2$ (N/m$^2$) |
| R | free-stream Reynolds number, $\frac{Vl\rho}{\mu}$ |
| S | wing reference area, ft$^2$ (m$^2$) |
| V | true airspeed, ft/sec (m/sec) |
| W | airplane weight, lb (kg) |
| $\alpha$ | angle of attack, deg |
| $\Delta$ | incremental increase |
| $\mu$ | absolute viscosity, lb-sec/ft$^2$ (N-sec/m$^2$) |
| $\rho$ | air density, slugs/ft$^3$ (kg/m$^3$) |

Subscripts:

| | |
|---|---|
| b | base |
| corr | corrected for sweep |

| | |
|---|---|
| f | friction |
| fb | forebody |
| ht | horizontal tail |
| le | leading edge |
| lvt | modified fixed ventral fin |
| max | maximum |
| uvt | upper vertical tail |
| w | wetted area |

## AIRPLANE

The modified X-15-2 is a single-place, low-aspect-ratio monoplane designed for manned flight research at Mach numbers near 8.0. The modifications included adding two jettisonable external propellant tanks, extending the fuselage by inserting a 29-inch (0.74-meter) section, and adding an external helium storage tank at the base of the upper vertical tail. Other changes included reducing the glass area in the cockpit canopy, extending the side fairings to the rear of the fuselage to provide additional hydrogen-peroxide storage space, and extending the nose gear and main gear to allow clearance for emergency landings with an attached ramjet engine.

The X-15-2 airplane was carried aloft under the right wing of a B-52 airplane and launched at an altitude of approximately 45,000 feet (13,716 meters) at a Mach number of approximately 0.8. It was powered by a rocket engine to fuel cutoff or exhaustion and then glided back to a lakebed landing at Edwards Air Force Base, Calif.

A three-view drawing of the modified X-15-2 airplane with the lower ventral fin attached is shown in figure 1(a).[1] Physical characteristics of the airplane are presented in table 1. Figure 1(b) shows the modified X-15-2 airplane with the dummy ramjet, which was flown on the last three flights considered in this study. The dummy ramjet was mounted in the position formerly occupied by the lower ventral fin. Details of the modified fixed portion of the ventral fin and the dummy ramjet are presented in reference 5.

For the last two flights of this study, all the wetted surfaces of the airplane were sprayed with an ablative except the leading-edge surfaces, on which preformed ablative sections were used. A flight evaluation of the ablative coating and a discussion of the application and refurbishment techniques are presented in reference 6.

[1]The two external drop tanks were jettisoned during the ascent (powered) portion of flight at approximately Mach 2 and are, therefore, not a part of this study. Details of the jettisonable tanks and their drag are presented in reference 4.

TABLE 1.– PHYSICAL CHARACTERISTICS OF THE X-15-2 AIRPLANE

| | |
|---|---|
| Wing – | |
| Airfoil section | NACA 66005 (modified) |
| Total area (includes 94.98 $ft^2$ (8.82 $m^2$) covered by fuselage), $ft^2$ ($m^2$) | 200 (18.6) |
| Span, ft (m) | 22.36 (6.82) |
| Mean aerodynamic chord, ft (m) | 10.27 (3.13) |
| Root chord, ft (m) | 14.91 (4.54) |
| Tip chord, ft (m) | 2.98 (0.91) |
| Taper ratio | 0.20 |
| Aspect ratio | 2.50 |
| Sweep at 25-percent-chord line, deg | 25.64 |
| Incidence, deg | 0 |
| Dihedral, deg | 0 |
| Aerodynamic twist, deg | 0 |
| Horizontal tail – | |
| Airfoil section | NACA 66005 (modified) |
| Total area (includes 63.29 $ft^2$ (5.88 $m^2$) covered by fuselage), $ft^2$ ($m^2$) | 115.34 (10.7) |
| Span, ft (m) | 18.08 (5.51) |
| Mean aerodynamic chord, ft (m) | 7.05 (2.15) |
| Root chord, ft (m) | 10.22 (3.12) |
| Tip chord, ft (m) | 2.11 (0.64) |
| Taper ratio | 0.21 |
| Aspect ratio | 2.83 |
| Sweep at 25-percent-chord line, deg | 45 |
| Dihedral, deg | -15 |
| Upper vertical tail – | |
| Airfoil section | 10° single wedge |
| Total area, $ft^2$ ($m^2$) | 40.91 (3.8) |
| Span, ft (m) | 4.58 (1.40) |
| Mean aerodynamic chord, ft (m) | 8.95 (2.73) |
| Root chord, ft (m) | 10.21 (3.11) |
| Tip chord, ft (m) | 7.56 (2.30) |
| Taper ratio | 0.74 |
| Aspect ratio | 0.51 |
| Sweep at 25-percent-chord line, deg | 23.41 |
| Lower vertical tail – | |
| Airfoil section | 10° single wedge |
| Total area, $ft^2$ ($m^2$) | 34.41 (3.2) |
| Span, ft (m) | 3.83 (1.17) |
| Mean aerodynamic chord, ft (m) | 9.17 (2.80) |
| Root chord, ft (m) | 10.21 (3.11) |
| Tip chord, ft (m) | 8 (2.44) |
| Taper ratio | 0.78 |
| Aspect ratio | 0.43 |
| Sweep at 25-percent-chord line, deg | 23.41 |
| Movable (jettisonable portion) surface area, $ft^2$ ($m^2$) | 19.95 (1.85) |
| Fuselage – | |
| Length, ft (m) | 51.59 (15.72) |
| Maximum width, ft (m) | 7.33 (2.23) |
| Maximum depth, ft (m) | 4.67 (1.42) |
| Maximum depth over canopy, ft (m) | 4.97 (1.51) |
| Side area (total), $ft^2$ ($m^2$) | 221.38 (20.6) |

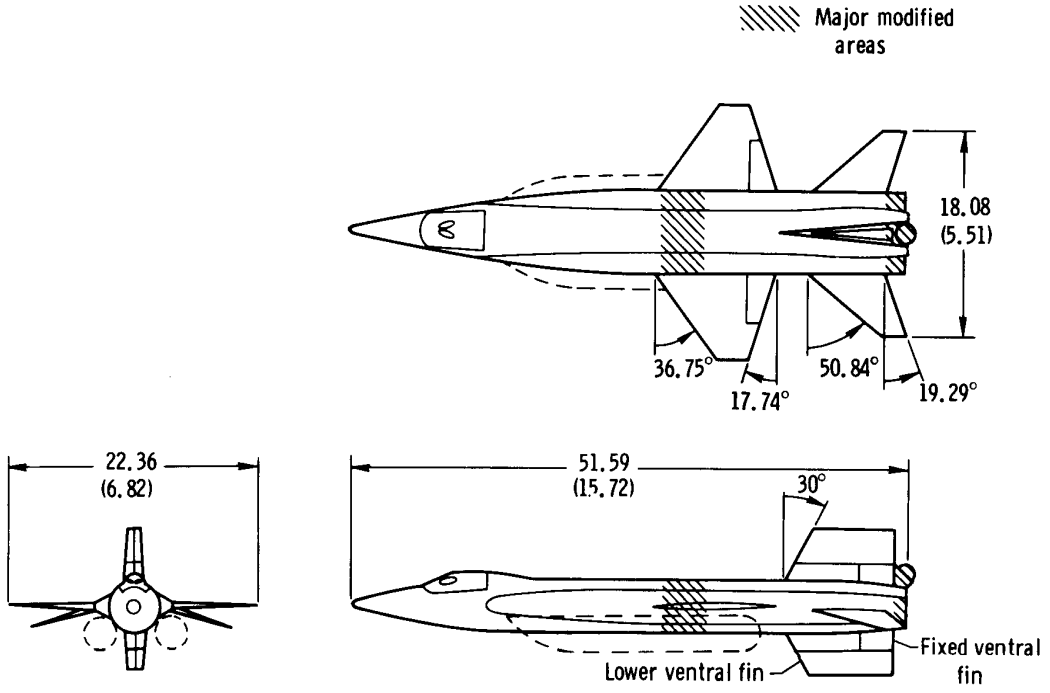


*(a) Modified airplane with lower ventral fin. (Location of jettisonable tanks shown with dashed lines.)*

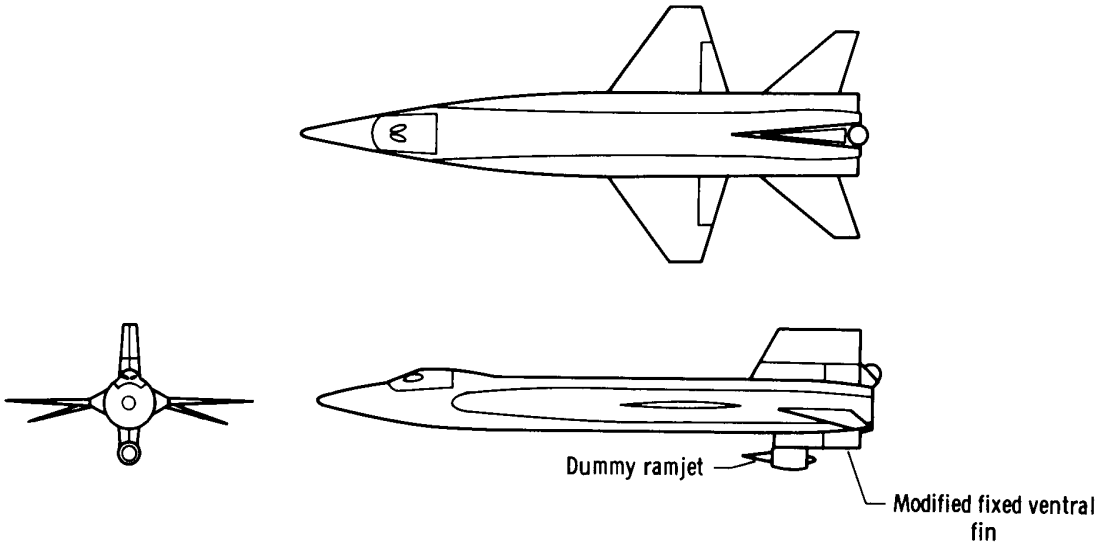


*(b) Modified airplane with modified fixed ventral fin and dummy ramjet.*

*Figure 1. Three-view drawings of modified X-15-2 airplane. Dimensions in feet (meters) unless otherwise noted.*

## METHODS

The accelerometer method (described in ref. 7) was used to determine total lift and drag. In this method lift and drag for the power-off conditions are calculated by using the following relationships:

$$L = (a_n \cos \alpha + a_l \sin \alpha)\frac{W}{g}$$

$$D = (a_n \sin \alpha - a_l \cos \alpha)\frac{W}{g}$$

$$C_L = \frac{L}{qS}$$

$$C_D = \frac{D}{qS}$$

$$L/D = \frac{C_L}{C_D} = \frac{a_n \cos \alpha + a_l \sin \alpha}{a_n \sin \alpha - a_l \cos \alpha}$$

The base pressure coefficients were determined from the following relationship:

$$C_{p_b} = \frac{p_b - p}{q}$$

The incremental drag associated with any component or configuration was determined by comparing the total drag of the modified airplane in the various configurations and, in some cases, by comparing it with the total drag of the basic configuration of reference 2. The simple technique that was used to predict the increase in drag coefficient caused by the ablative coating is presented in the appendix.

## INSTRUMENTATION

The parameters used to determine lift and drag were recorded with an NACA internal recording system. Accelerometers were positioned within 21 inches (0.53 meters) of the airplane center of gravity. Angle of attack and angle of sideslip were obtained from the hypersonic flow-direction sensor, or ball nose (ref. 8). Radar tracking and radiosonde data provided Mach number and ambient pressure. References 9 and 10 discuss the methods used to obtain Mach number and dynamic and static pressure.

A standard NACA 12-cell, photorecording manometer was used to measure base pressure. The two orifice locations are shown in figure 2.

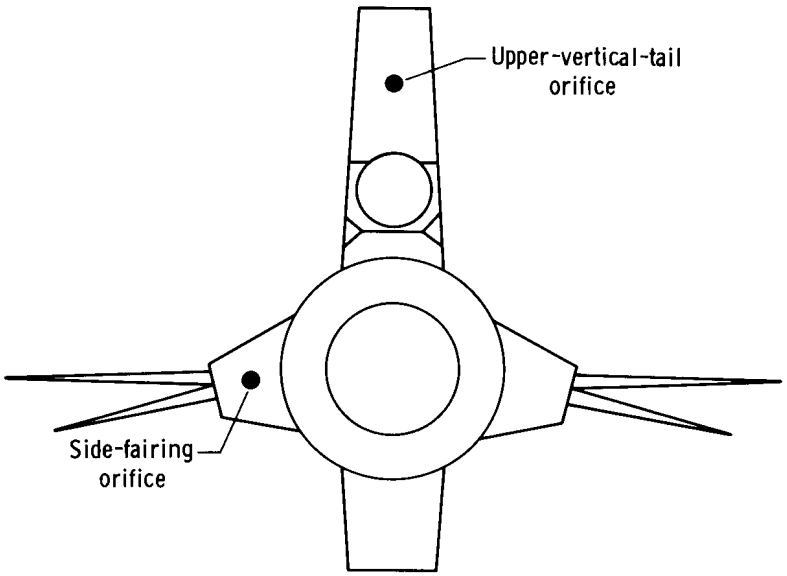


*Figure 2. Sketch of X-15 base showing locations of orifices.*

Aircraft weight was determined by integrating the fuel flow rates against time and subtracting the fuel used from the initial known fuel weights in the tanks.

## TEST CONDITIONS

Data presented in this paper were obtained during the trimmed, power-off portions of flight in which the speed brakes were closed. The Mach number ranged from about 0.5 to 6.7, with free-stream Reynolds numbers of approximately $1.7 \times 10^8$ to $3.6 \times 10^7$ based on fuselage length. The angle of attack ranged from 0° to 11°, whereas the angle of sideslip was maintained at negligible values. The altitude varied from approximately 3000 feet (914 meters) to 102,000 feet (31,090 meters), and the dynamic pressure ranged from about 300 lb/ft$^2$ (14,364 N/m$^2$) to 770 lb/ft$^2$ (36,868 N/m$^2$). The flow was considered to be turbulent over essentially the entire wetted surface of the aircraft.

The number of flights made with the various modified X-15-2 configurations on which data were obtained for this paper were as follows:

| Configuration | Number of flights |
|---|---|
| Clean (no ablative) | |
| Lower ventral fin on | 5 |
| Lower ventral fin off | 14 |
| Dummy ramjet on | 1 |
| Coated (with ablative) | |
| Dummy ramjet on | 2 |

For the last flight of this study, on which the highest Mach number was reached, only data obtained immediately following burnout and before the modified fixed ventral fin (pylon) and dummy ramjet were damaged are presented. Holes were burned in the pylon, as a result of complex shock impingement and interference effects (ref. 11), which were large enough to cause significant additional drag. Instrumentation on the pylon indicated that most of the damage occurred several seconds after the maximum Mach number was obtained.

## ACCURACY

The instrumentation and techniques used to calculate lift and drag coefficients for the modified X-15-2 airplane were the same as those used in reference 2. The maximum errors of the parameters for Mach numbers between 1 and 6 and altitudes below 100,000 feet (30,480 meters) were as follows:

| Parameter | Error |
|---|---|
| $a_l$ | ±0.005g |
| $a_n$ | ±0.05g |
| $\alpha$ | ±1.0° |
| M | ±0.05 |
| p | ±6 lb/ft$^2$ (287.20 N/m$^2$) |
| W | ±200 lb (90.72 kg) |
| $p_b$ | ±4 lb/ft$^2$ (191.52 N/m$^2$) |
| q | ±0.05q |

Most of these errors tend to be random in both sign and magnitude; therefore, the overall error in the lift and drag coefficients would also tend to be random.

The maximum estimated error in drag coefficient attributed to the error in the various parameters was:

| Parameter | $\frac{\Delta C_D}{C_D}$, percent |
|---|---|
| $a_l$ | ±2 |
| $a_n$ | ±2 |
| $\alpha$ | ±4 |
| M | ±3 |
| W | ±1 |
| q | ±1 |
| Root-sum-square error | ±6 |

The root-sum-square error in drag coefficient is reduced when the data are plotted and faired with respect to Mach number.

Most of the scatter in the computed flight data is due to the limited ranges of lift coefficient, drag coefficient, and angle of attack over which data were obtained. In spite of these limitations, the summary plots presented are believed to show reliably the trends caused by the modifications.

Lift coefficients were also obtained from faired flight results and are within ±4 percent of the values shown. The error in lift-to-drag ratio associated with the errors in lift coefficient and drag coefficient is approximately ±7 percent. For the base pressure coefficient, the maximum estimated error $\left(\frac{\Delta C_{p_b}}{C_{p_b}}\right)$ in the flight data is ±8 percent (ref. 12).

## DISCUSSION OF RESULTS

### Clean-Configuration Drag

The flight drag coefficients for the modified X-15-2 clean configuration, with and without the lower ventral fin, for lift coefficients from 0 to 0.3 are shown in figure 3(a). Most of these data show the additional drag caused by the lower ventral fin. The incremental difference in drag coefficient between the lower-ventral-fin-on and off data increases as the lift coefficient increases between 0.1 and 0.3. At zero-lift coefficient no change in drag coefficient is definable from the available data. The drag of the lower ventral fin is discussed further in a later section.

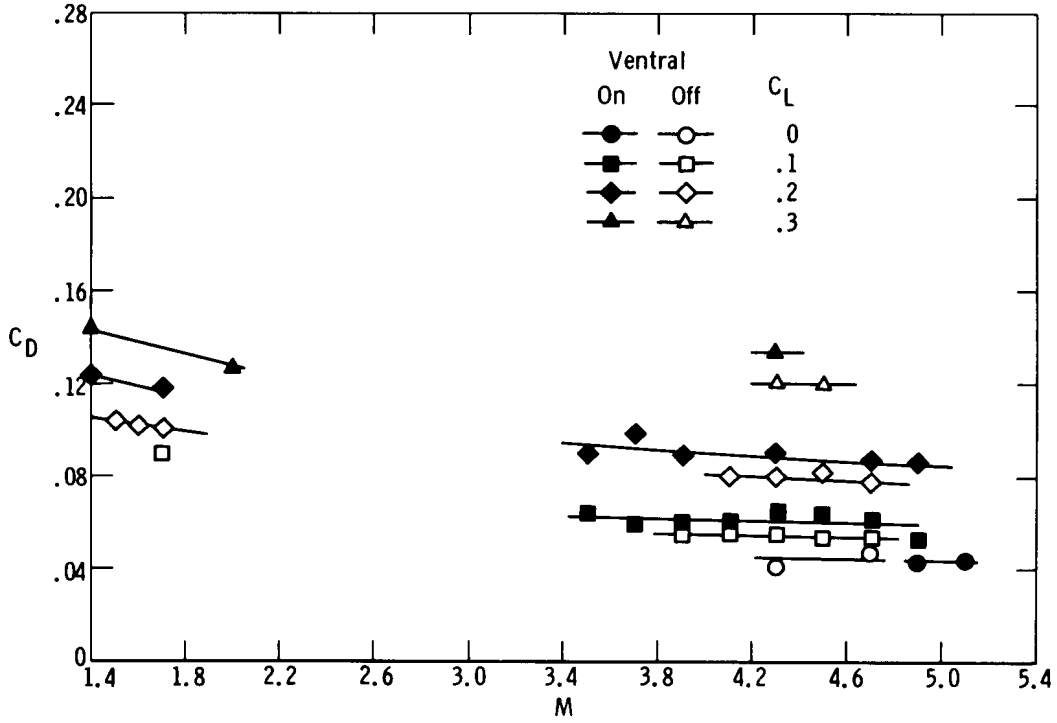


*(a) Modified airplane with lower ventral fin on and off.*

*Figure 3. Variation of total airplane drag coefficient with Mach number for constant values of lift coefficient. Clean (no ablative) configuration.*

Figure 3(b) compares the faired data of figure 3(a) for the modified X-15-2 ventral-fin-on configuration with the flight results for the basic (unmodified) airplane (ref. 2 and unpublished flight data) to note the effects of the airframe modifications. The differences in drag coefficient between the modified X-15-2 and the basic unmodified aircraft are, in general, small and seem to be independent of lift coefficient. Thus the drag coefficients for the modified X-15-2 clean configuration did not change significantly from those for the basic X-15 airplane.

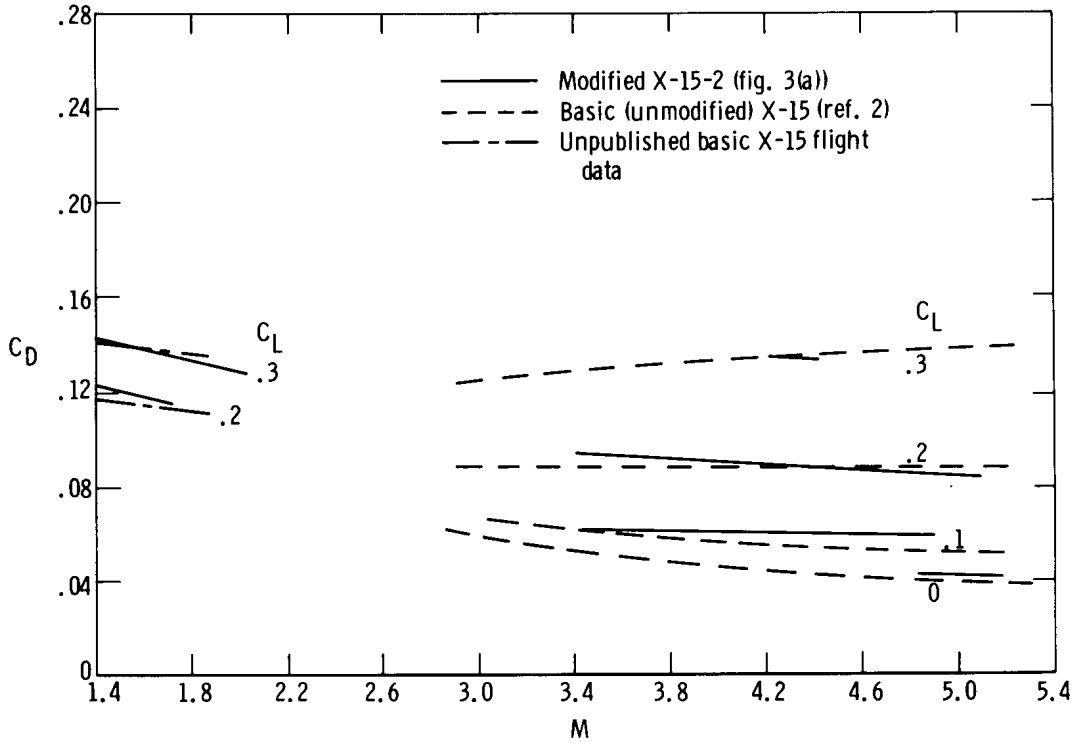


*(b) Modified and basic airplane with the lower ventral fin on.*

*Figure 3. Concluded.*

Figure 4 compares the flight drag coefficients of the clean configuration with the lower ventral fin on to those of the clean configuration with the dummy ramjet installed. The data show an average increase in supersonic drag coefficient for the dummy ramjet of about 0.008 at lift coefficients between 0 and 0.2 relative to the lower-ventral-fin data. The difference between the two configurations tends to decrease with increasing lift coefficient. At $C_L = 0.3$, the available data for the two configurations appear to converge.

## Coated-Configuration Drag

Drag coefficients for the ablative-coated and clean configurations with the dummy ramjet on are shown in figure 5. The drag coefficients for the coated configuration are greater than those for the clean configuration, and the difference in coefficient between the two configurations tends to increase with increasing lift coefficient.

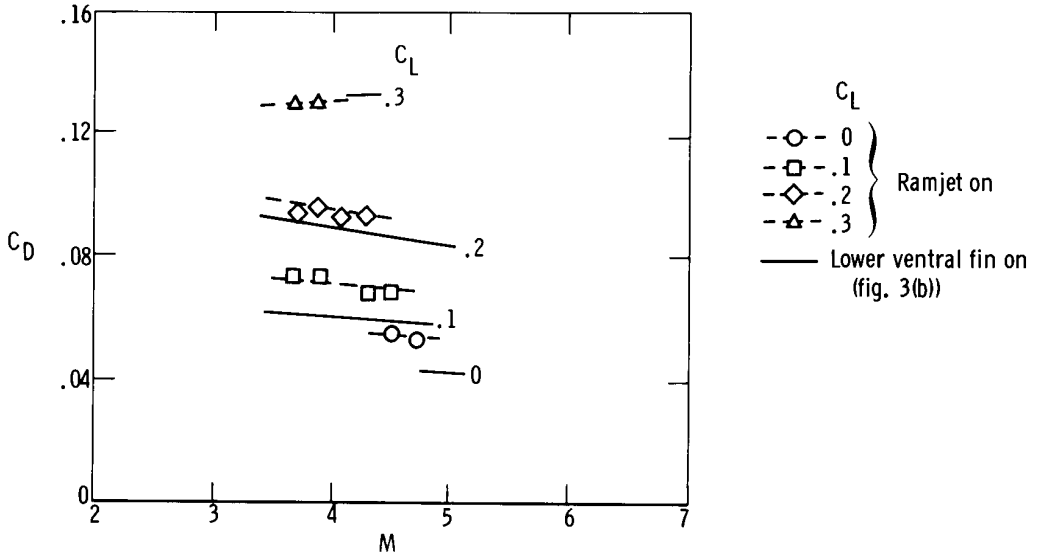


*Figure 4. Flight drag coefficients of clean configuration with the dummy ramjet or the lower ventral fin on as a function of Mach number.*

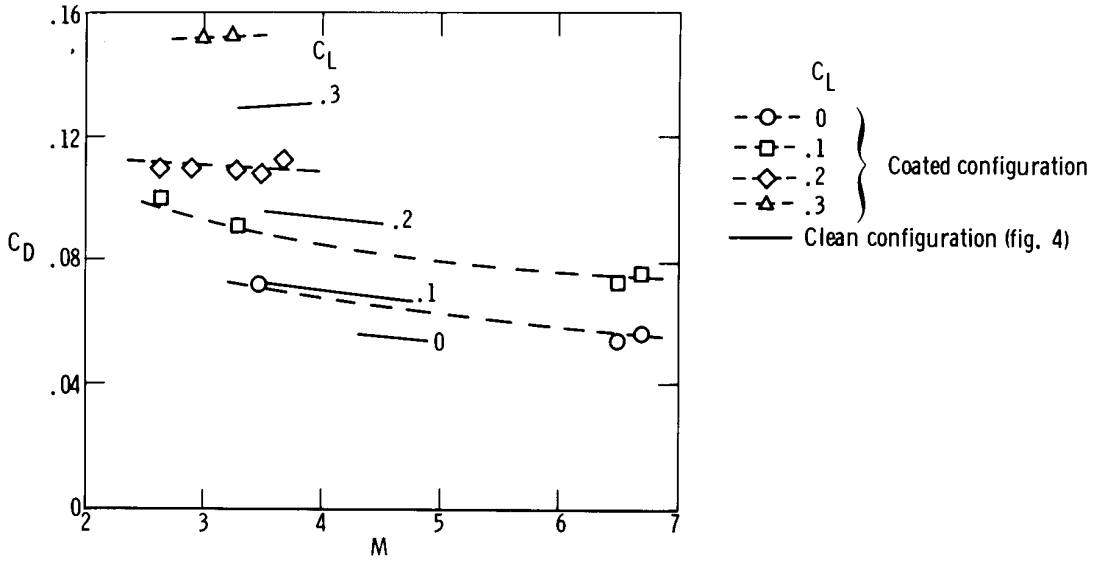


*Figure 5. Flight drag coefficients for the coated and clean configurations with the dummy ramjet on as a function of Mach number.*

Another way of presenting the incremental increase in drag coefficient due to the ablative coating and the dummy ramjet over that for the clean configuration with the lower ventral fin on is shown in figure 6. These selected flight incremental values cover the Mach range from 3.0 to 5.0 and are based on the faired data of figures 4 and 5. As lift coefficient increases from 0 to 0.3, the incremental drag of the ramjet decreases while the incremental drag of the ablative coating increases. At $C_L = 0.1$ (fig. 6(b)) the incremental increase in drag of the dummy ramjet and ablative coating are about equal.

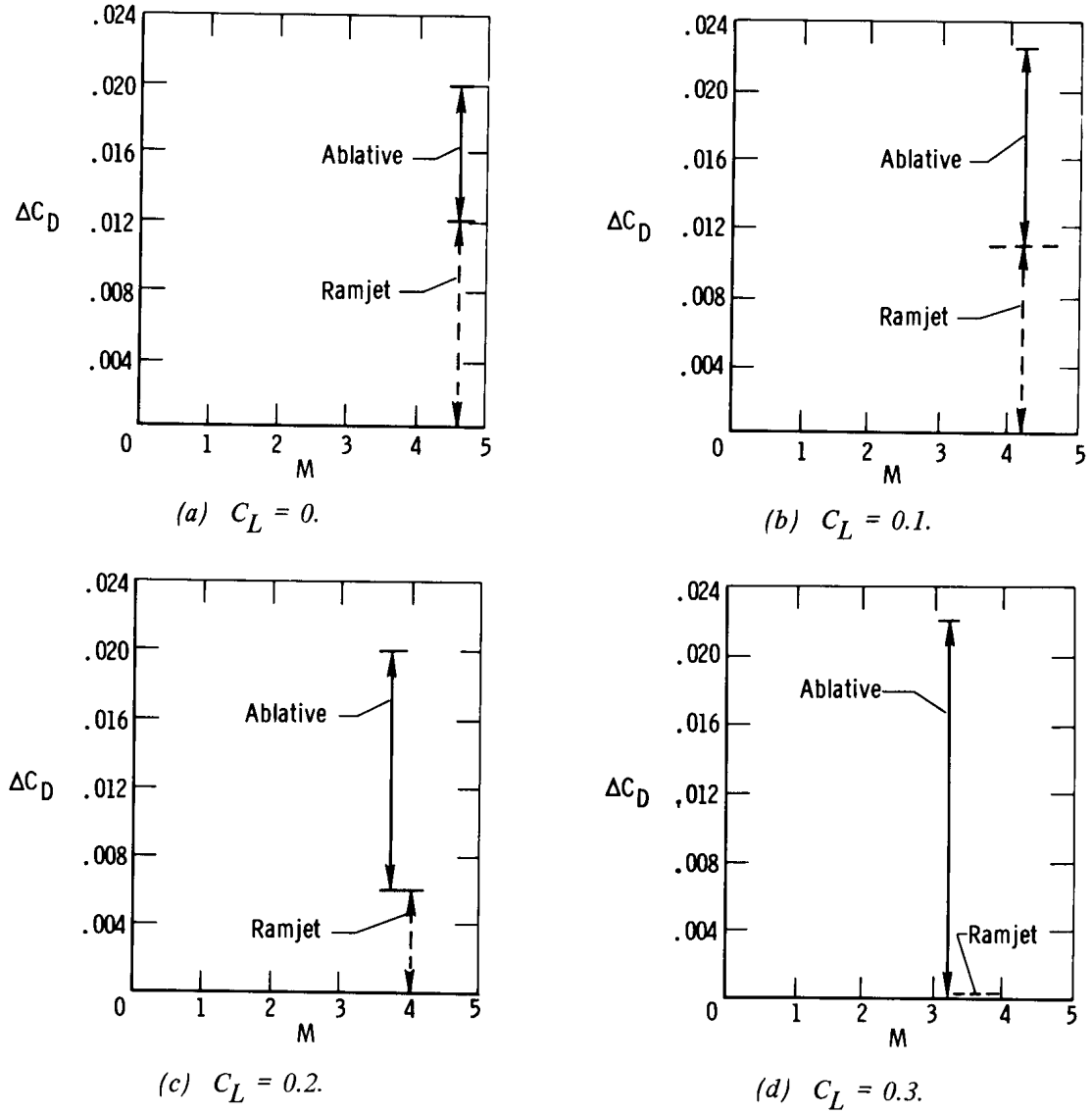


*Figure 6. Incremental increase in drag over the clean configuration with the lower ventral fin on due to the ablative coating and dummy ramjet as a function of Mach number.*

Figure 7 compares the flight incremental increase in drag coefficient due to the ablative coating (crosshatched regions) with predicted values derived by the methods described in the appendix. The supersonic flight values were obtained from the data of figure 6. As shown, the ablative coating increased the supersonic drag coefficient about 0.008 at $C_L = 0$ and about 0.022 at $C_L = 0.3$. This increase, at the lowest lift coefficient, can be attributed to the increased roughness, increased leading-edge diameters, and larger base areas resulting from the ablative coating.

The subsonic data in figure 7 that were not included in the previous figures are for lift coefficients of 0.3 and 0.4, with the higher drag values again being for higher lift coefficient. These data show an average increase in the subsonic drag coefficient of 0.013 for lift coefficients of 0.3 and 0.4.

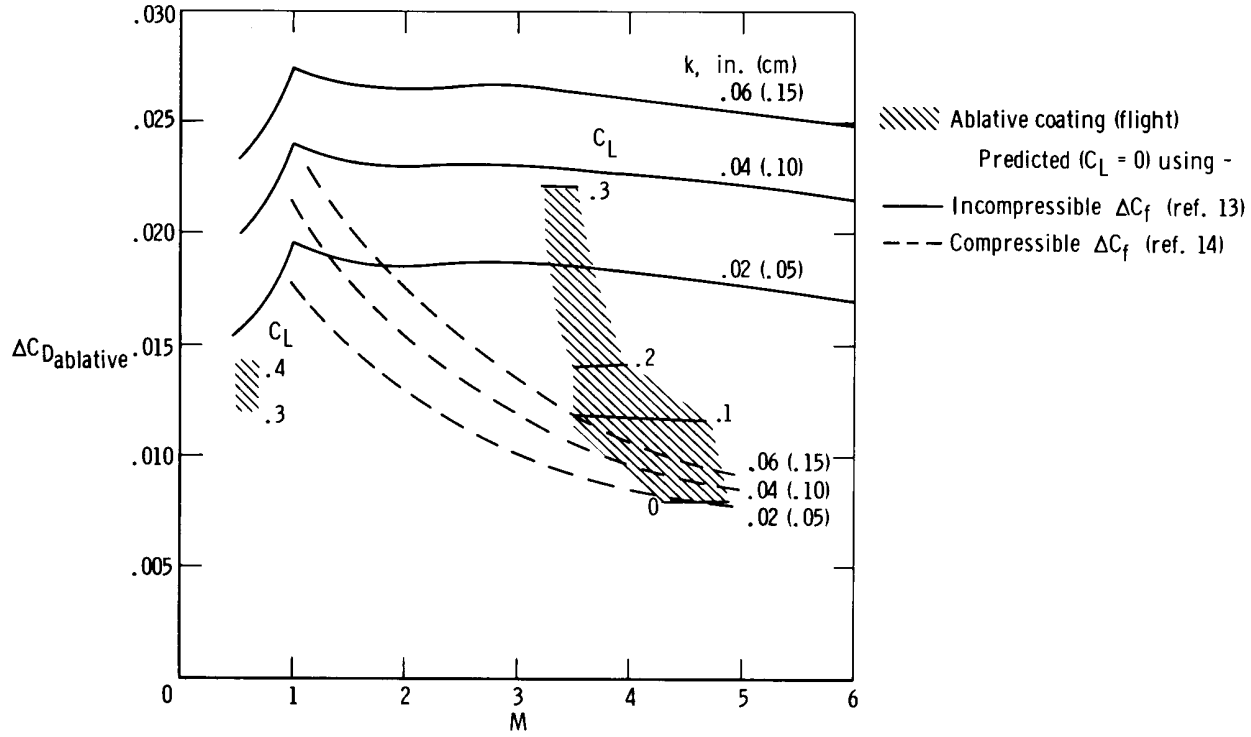


*Figure 7. Variation of the flight incremental drag coefficient caused by the ablative coating as a function of Mach number. k = 0.04 in. (0.10 cm).*

The methods used to predict the increased drag coefficient resulting from the ablative coating are presented in the appendix. The predicted values presented in figure 7 include both incompressible (ref. 13) and compressible (ref. 14) skin-friction drag coefficients. The predicted values include base drag coefficients and leading-edge drag coefficients that were adjusted for compressible effects.

As shown in figure 7, the supersonic flight data at $C_L = 0$ agree well with the predicted values for the compressible skin-friction coefficients for a flat plate at zero incidence (ref. 14), where the flight-estimated average roughness height k of the coating after ablative action was 0.04 inch (0.10 centimeter). As the lift coefficient increases, the flight incremental drag coefficient also increases and begins to deviate from the predicted compressible skin-friction coefficient. This increase in $\Delta C_{D_{ablative}}$ with lift is consistent with wind-tunnel results for the effect of roughness on the drag of the X-24 lifting body in reference 15. Although the configurations differ, these results, including the present findings, suggest that, with increasing angle of attack, or lift, the aft upper-surface regions of the vehicle experience a growing area of separated flow.

## Lower-Ventral-Fin Drag

A breakdown of the predicted drag-component increments of the lower ventral fin is presented in figure 8. These predicted values are based on free-stream conditions (isolated lower ventral fin) and were obtained by using a buildup method with data from reference 16. The following relationship was applied to obtain the predicted values:

$$\Delta C_{D_{\text{lower ventral fin}}} = \Delta C_{D_{le}} + \Delta C_{D_{fb}} + \Delta C_{D_b} + \Delta C_{D_f}$$

where the forebody incremental drag coefficients $\Delta C_{D_{fb}}$ above Mach 1.6 were obtained by using the transonic similarity rule (ref. 16). The total predicted drag coefficient decreases from a transonic value near 0.010 to a value near 0.003 at Mach 5.

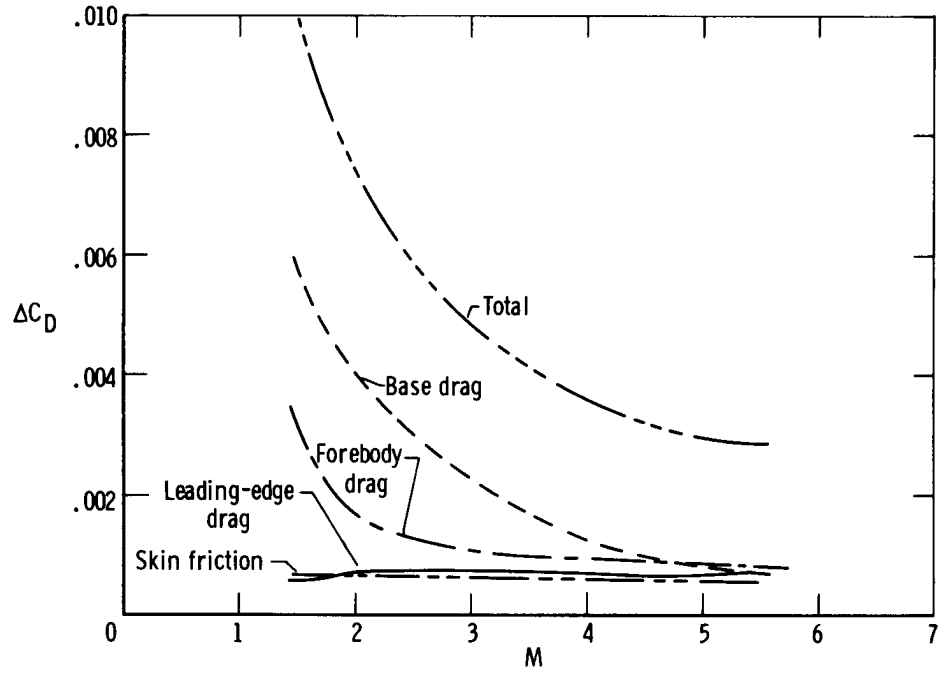


*Figure 8. Predicted drag-component increments for the lower ventral fin as a function of Mach number.*

The flight-determined increment of drag caused by the lower ventral fin (fig. 3(a)) is compared in figure 9 with predicted values and unpublished wind-tunnel data. The

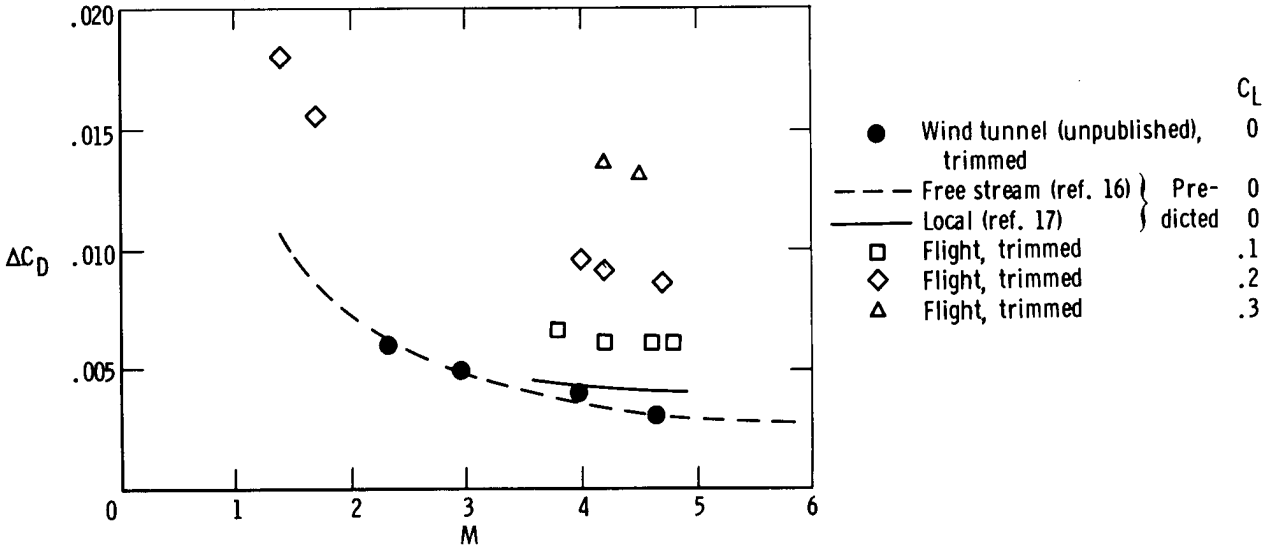


*Figure 9. Incremental drag coefficients of the lower ventral fin as a function of Mach number.*

predicted values for the local conditions (lower ventral fin in the flow field of the X-15) were obtained by applying an adjustment to the free-stream predicted values (fig. 8), which were based on data from reference 17, to account for the difference in local dynamic pressure.

The predicted supersonic values using free-stream conditions and the wind-tunnel data in figure 9 show good agreement at zero-lift coefficient, but the predicted values using local conditions are slightly higher. The flight $\Delta C_D$ data increase with increasing lift coefficient, which suggests an increase in trim drag associated with the various lifting conditions and, possibly, interference effects which were not considered in the predictions. The flight incremental increase in drag coefficient of the lower ventral fin between Mach 3.8 and 4.9 was about 0.006 at a lift coefficient of 0.1 and 0.014 at a lift coefficient of 0.3.

When the lower ventral fin or the dummy ramjet was jettisoned at subsonic Mach numbers, an incremental value of $C_D$ due to the lower ventral fin or the dummy ramjet was obtained. The flight values are compared with predicted values in figure 10.

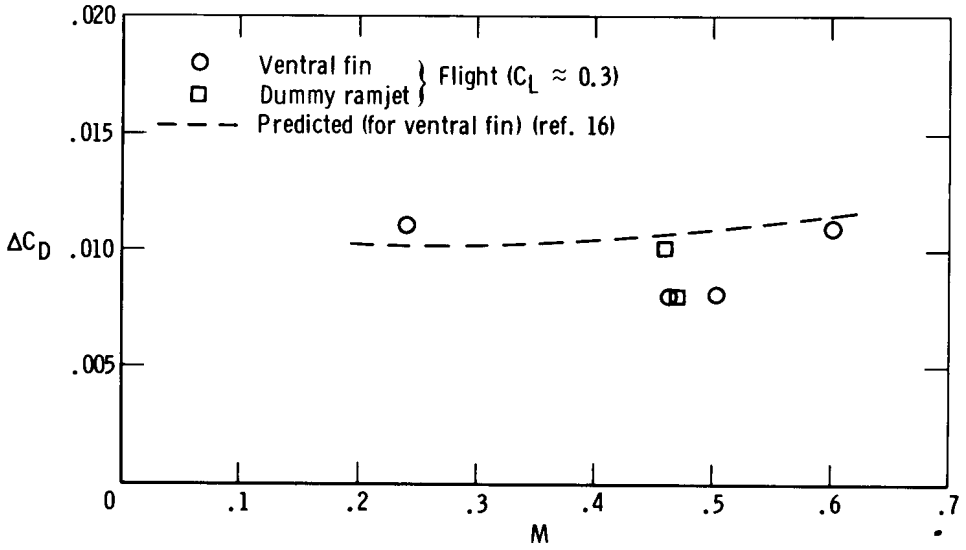


*Figure 10. Subsonic incremental values of airplane drag coefficient obtained after the lower ventral fin or dummy ramjet was jettisoned.*

The average increase in subsonic drag coefficient for the lower ventral fin and dummy ramjet was approximately 0.010 at a lift coefficient of about 0.3. The flight incremental drag values were obtained by determining the difference in total airplane drag coefficient just before and just after the lower ventral fin or the dummy ramjet was jettisoned. The incremental flight levels of drag coefficient for both the lower ventral fin and the dummy ramjet are similar and show fair agreement with predicted values. This similarity was not surprising, since the drag at subsonic speeds is primarily influenced by the base drag, the base areas of the ventral fin and the ramjet are within 6 percent of being equal, and the locations were similar.

## Lift-Drag Ratio

The variation of the maximum lift-drag ratio with Mach number for the various configurations of the modified X-15-2 airplane is presented in figure 11 and compared with data for the unmodified airplane. The data for the modified clean configuration with the lower ventral fin on agree with the comparable basic data from reference 2. The increase in $(L/D)_{max}$ at supersonic speeds for the modified clean configuration with the ventral fin off is attributed to the reduced drag resulting from the absence of the lower ventral fin. For the coated configuration, the level of most of the data shows a lower $(L/D)_{max}$ as a result of the increased drag, as discussed in a previous section.

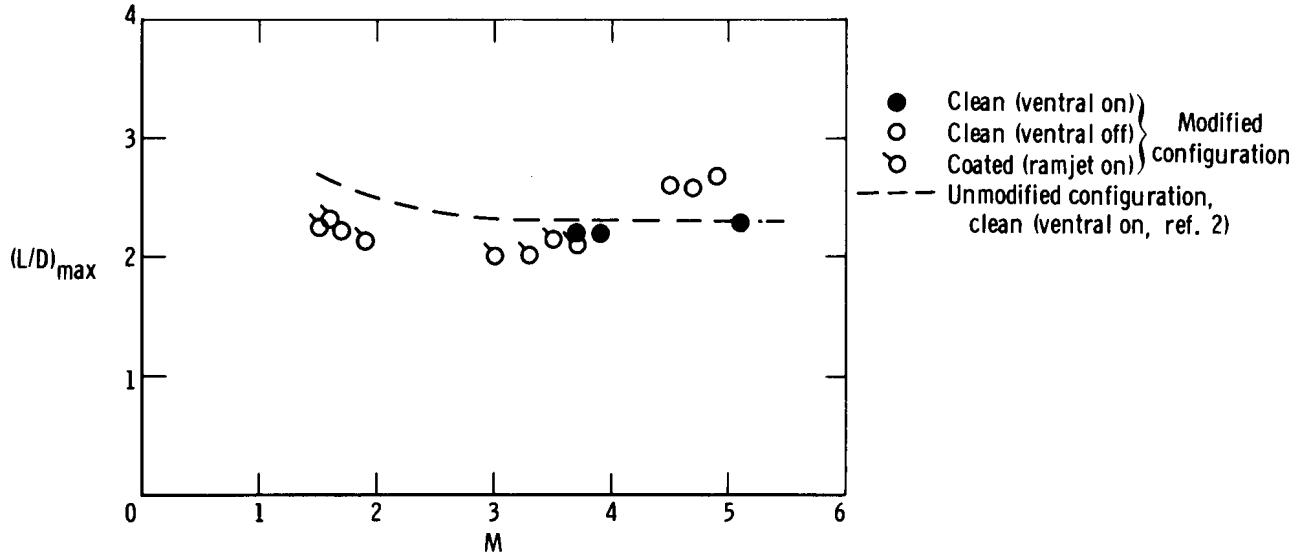


*Figure 11. Variation of maximum lift-drag ratio with Mach number. Trimmed flight.*

## Base Drag

In-flight base pressure measurements were made to determine the effects of adding an external helium storage tank at the base of the upper vertical tail and increasing the length of the side fairings when the X-15-2 airplane was modified. Because of practical limitations, not as many base pressure measurements were made as would have been desirable to determine whether the helium storage tank had an effect on the overall base drag. However, wind-tunnel tests and the flight data of reference 12 show that local effects are propagated throughout the base region. Thus, if the tank had a significant effect, the orifice on the upper vertical tail would be expected to sense it. The base pressure results for the upper vertical tail and the side fairing are shown in figure 12. Figure 12(a) presents the results for the center of the upper vertical tail, which agree well with the data of reference 12. This agreement shows that the tank had no measurable effect on the base drag of the upper vertical tail.

The side-fairing base pressure coefficients are presented in figure 12(b) and also show good agreement with the unmodified airplane data of reference 12 for Mach numbers greater than 2. For Mach numbers less than 2, the coefficients for the present

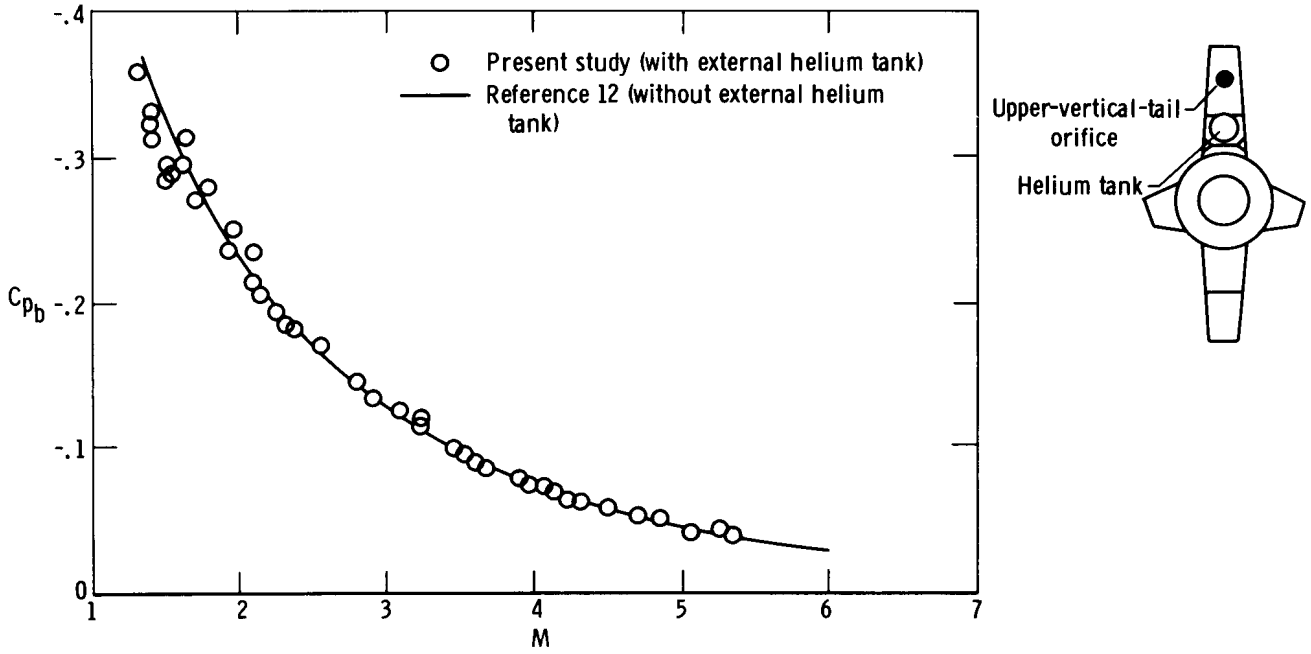


*(a) Center of upper vertical tail.*

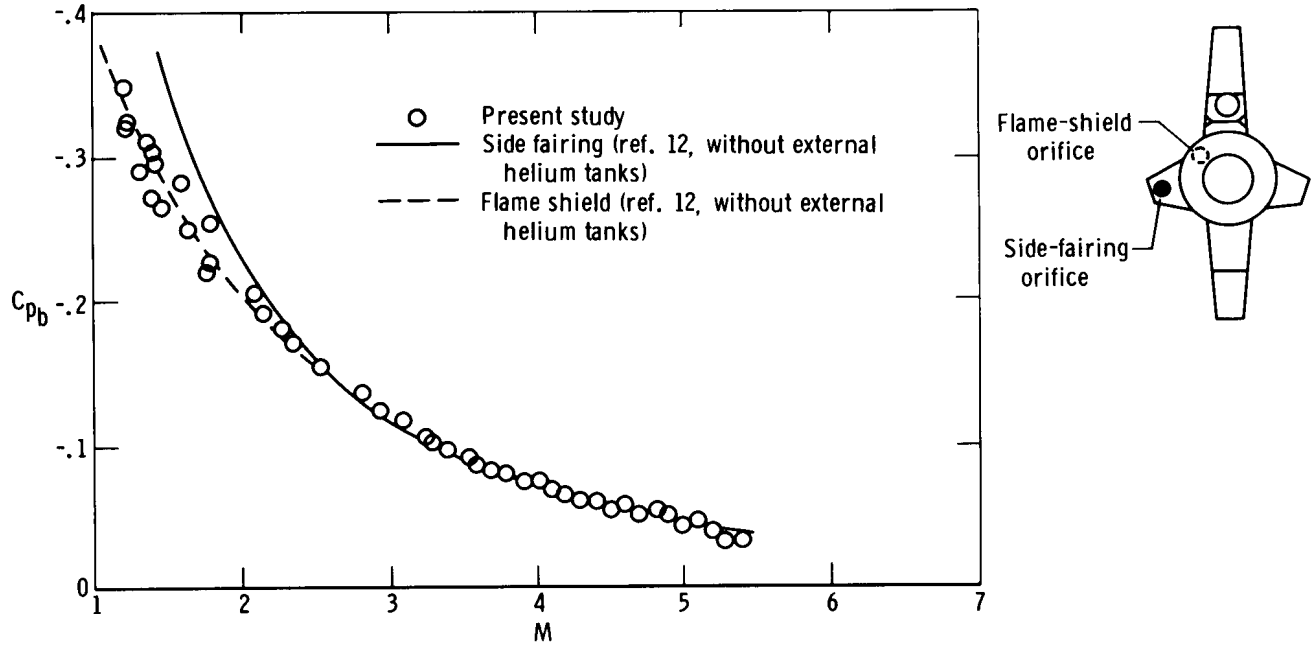


*(b) Side fairing.*

*Figure 12. Comparison of base pressure coefficients obtained from full-scale flight (power off) with and without the external helium tank.*

study tend to agree with the flame-shield data of reference 12. This was not surprising because the side fairings were extended so that their bases were adjacent to a large base (flame-shield base), which permitted the flame-shield and side-fairing base pressures to directly influence one another.

## CONCLUDING REMARKS

The modified X-15-2 airplane was flown with and without the lower ventral fin, dummy ramjet (including modified fixed ventral fin), and ablative coating. A study of the changes in drag characteristics for these various configurations yielded the following results:

The ablative coating increased the supersonic drag coefficient about 0.008 at a lift coefficient of 0 and 0.022 at a lift coefficient of 0.3. At subsonic speeds the average increase in drag coefficient was about 0.013 for lift coefficients of 0.3 and 0.4.

The flight incremental increase in drag coefficient of the lower ventral fin between Mach 3.8 and 4.9 was about 0.006 at a lift coefficient of 0.1 and 0.014 at a lift coefficient of 0.3. This increase in drag coefficient with increasing lift coefficient suggests an increase in trim drag and possibly interference effects. At subsonic speeds the flight increment showed fair agreement with predictions. The incremental increase in drag coefficient of the dummy ramjet at subsonic speeds was also about 0.010 at a lift coefficient of about 0.3.

Data for the modified X-15-2 airplane showed that the addition of an external helium tank at the base of the upper vertical fin had no measurable effect on the base pressure. Also, the extension of the fuselage side fairings so that their bases were adjacent to the fuselage base had no effect on the base pressure at Mach numbers above 2; however, at lower supersonic Mach numbers, the modified side-fairing base-pressure coefficients approached those of the flame-shield base.

The drag coefficients for the modified X-15-2 (clean configuration, lower ventral fin on) did not change significantly from those for the basic unmodified configuration.

**Flight Research Center,**
**National Aeronautics and Space Administration,**
**Edwards, Calif., April 15, 1970.**

# APPENDIX

## ESTIMATED ABLATIVE-COATING DRAG

The following simple techniques were used to estimate the increase in the drag coefficients caused by the ablative coating. Tables 2 and 3 show the dimensions used in the estimate. Typical examples of the surface roughness after ablative action are shown in figure 13.

TABLE 2. INCREMENTAL DIMENSIONS OF BASE AREAS AND LEADING EDGES AFTER ABLATIVE ADDITION

| | Base | | Leading edge | |
|---|---|---|---|---|
| | $\Delta d$, ft (m) | $\Delta A$, $ft^2$ ($m^2$) (a) | $\Delta d$, ft (m) | $\Delta A$, $ft^2$ ($m^2$) |
| Right wing | 0.010 (0.0030) | 0.0783 (0.00727) | 0.0700 (0.0213) | 0.5320 (0.04942) |
| Left wing | .013 (.0040) | .0978 (.00909) | .0700 (.0213) | .5320 (.04942) |
| Right horizontal tail | .018 (.0055) | .0958 (.00890) | .0708 (.0216) | .3879 (.03604) |
| Left horizontal tail | .018 (.0055) | .0958 (.00890) | .0708 (.0216) | .3879 (.03604) |
| Upper vertical tail | .028 (.0085) | .1290 (.01198) | .0466 (.0142) | .2134 (.01983) |
| Modified fixed ventral fin | .039 (.012) | .0562 (.00522) | .0466 (.0142) | .2134 (.01983) |

(a) Projected area.

TABLE 3. LENGTHS AND WETTED AREAS USED TO ESTIMATE ABLATIVE DRAG INCREMENT

| | Length, ft (m) | | | Wetted area, $ft^2$ ($m^2$) |
|---|---|---|---|---|
| | Leading edge (a) | Base | Mean chord | |
| Wings | 7.60 (2.32), each panel | 7.60 (2.32), each panel | 6.97 (2.12) | 211 (19.6), both panels |
| Horizontal tails | 5.48 (1.67), each panel | 5.48 (1.67), each panel | 4.56 (1.39) | 100 (9.29), both panels |
| Upper vertical tail | 4.58 (1.40) | 4.58 (1.40) | 8.8 (2.7) | 88 (8.2) |
| Modified fixed ventral fin | 1.45 (0.442) | 1.45 (0.442) | 9.13 (2.78) | 29 (2.7) |
| Fuselage | ---- -------- | ---- ------ | 51.59 (15.72) | 760 (70.6) |

(a) Projected length.

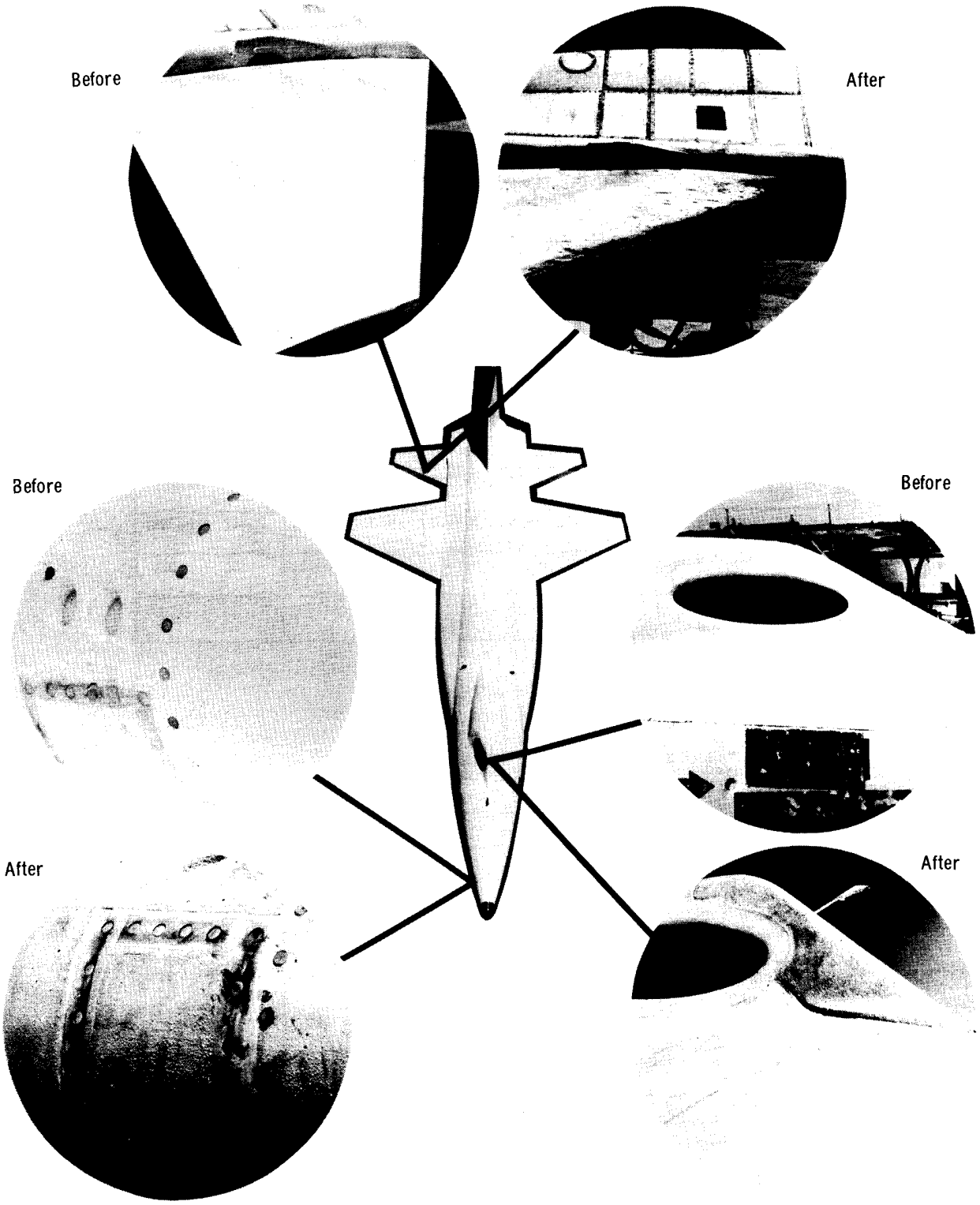


*Figure 13. Examples of the surface roughness on the modified X-15-2 airplane before and after ablative action.*

## APPENDIX

## ABLATIVE DRAG COEFFICIENT

The total estimated drag coefficient resulting from the applied ablative coating was obtained by using the following relationship:

$$\Delta C_{D_{ablative}} = \Delta C_{D_b} + \Delta C_{D_{le}} + \Delta C_{D_f} \quad \text{(fig. 7)}$$

### LEADING EDGES

The increase in drag coefficient from the increased leading-edge diameters was determined from the following relationship:

$$\Delta C_{D_{le}} = \frac{C_{D_c} \Delta d l}{S} = \frac{C_{D_c} \Delta A_{le}}{S}$$

where $l$ is the projected length, and $C_{D_c}$ was determined by subtracting the cylinder base drag coefficient from the cylinder drag coefficient. The cylinder drag coefficients were obtained from figure 14 (adapted from ref. 16), and corrections for sweep (angle

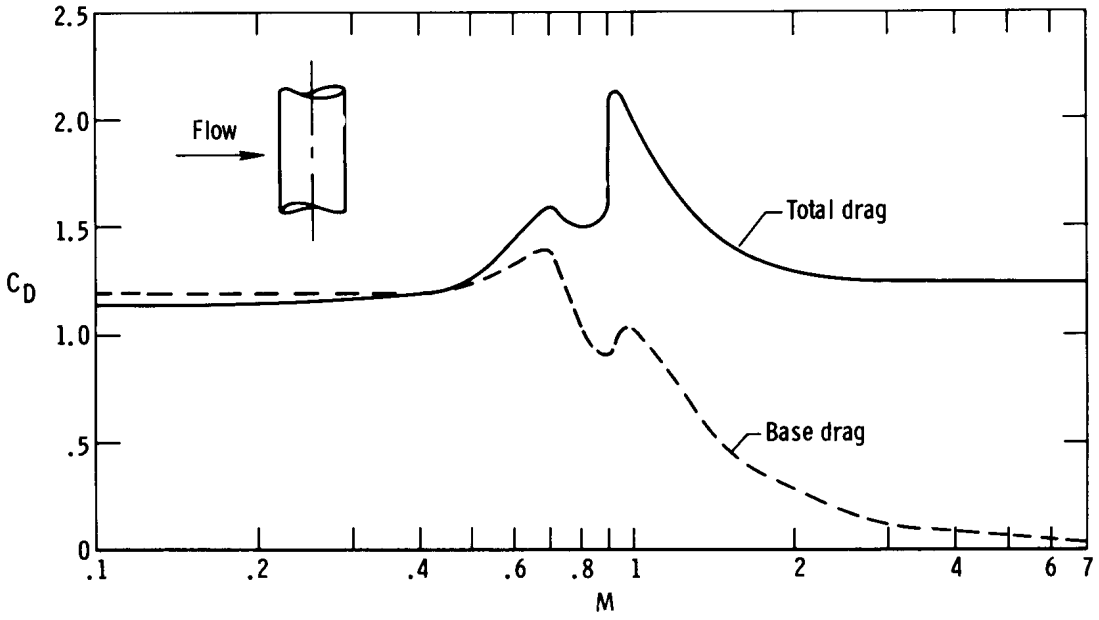


*Figure 14. Drag coefficient as a function of Mach number for a cylinder at $\alpha = 90^o$ (fig. 20 of ref. 16, page 16-16).*

of attack of a cylinder) were applied by using data in figure 15 (derived from refs. 16 and 18) and the following relationship:

$$\left(\Delta C_{D_{le}}\right)_{corr} = \frac{\left(C_D\right)_{sweep}}{\left(C_D\right)_{\alpha = 90°}} \left(\Delta C_{D_{le}}\right)$$

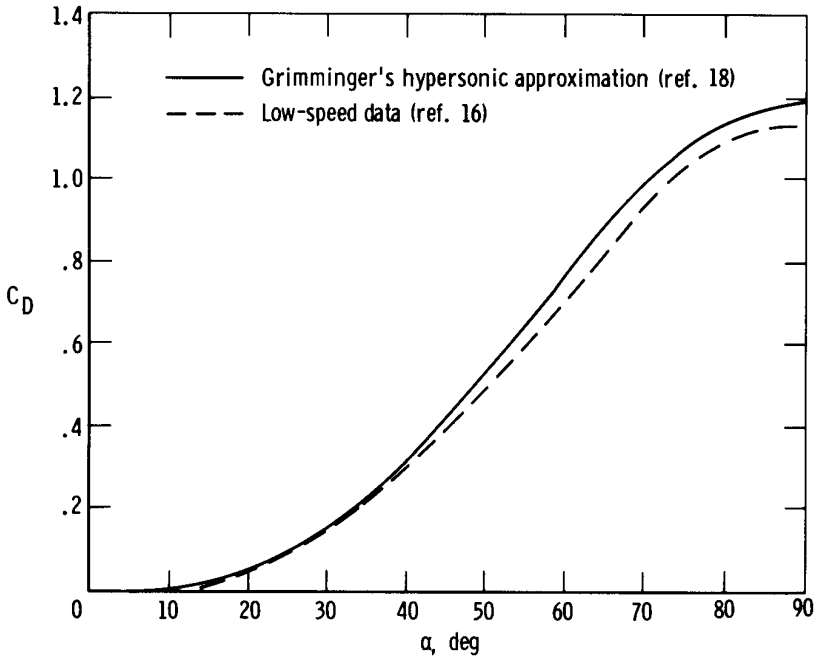


*Figure 15. Variation with angle of attack of the drag coefficient of a circular cylinder.*

The results are shown in figure 16.

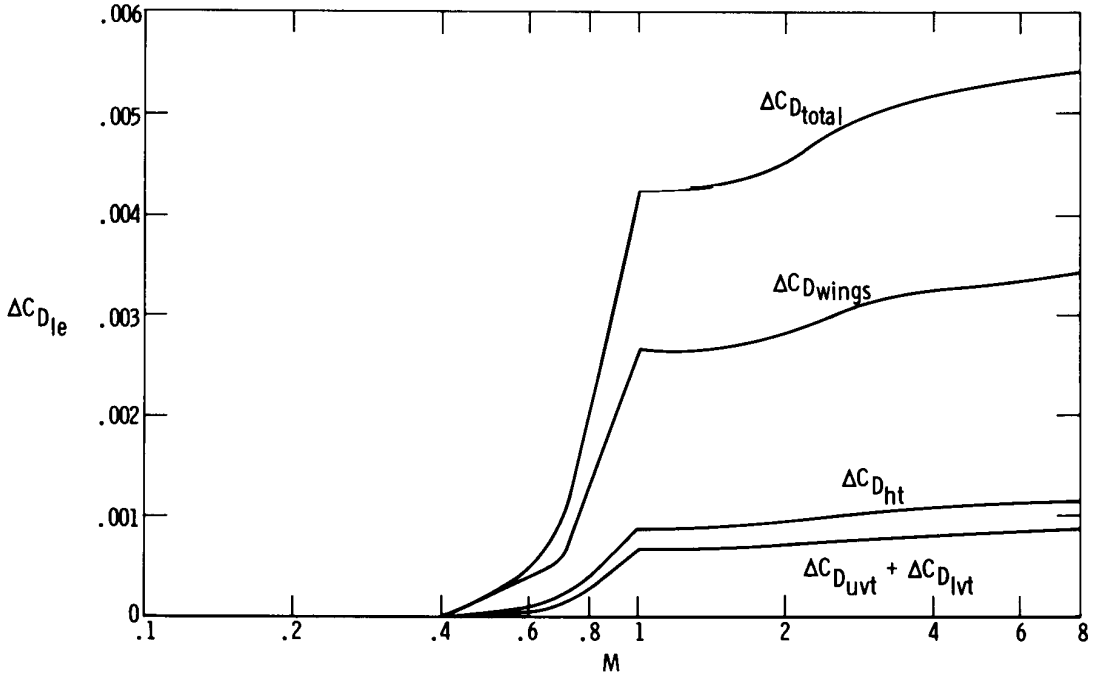


*Figure 16. Estimated increase in modified X-15-2 leading-edge drag coefficient caused by an applied ablative as a function of Mach number.*

## APPENDIX

## BASE DRAG COEFFICIENT

The incremental base drag coefficient caused by the increase in base areas from the applied ablative was determined by using the expression

$$\Delta C_{D_b} = \frac{C_{D_b} \Delta A_b}{S}$$

where $C_{D_b}$ was determined from figure 17 (derived from ref. 16). The results are

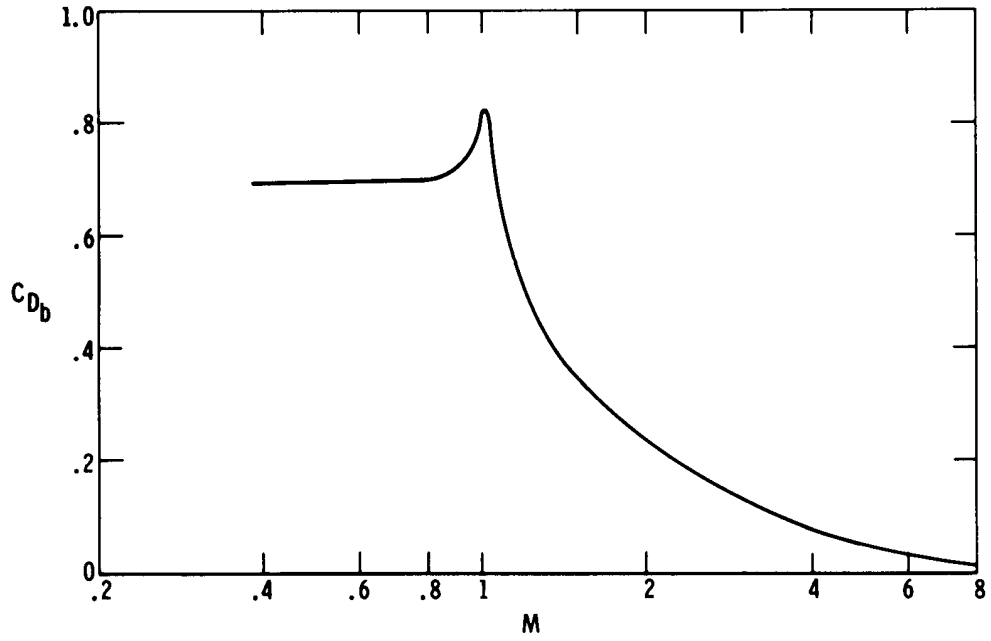


*Figure 17. Two-dimensional base drag originating from the blunt trailing edge of airfoil sections as a function of Mach number (fig. 11 of ref. 16, page 16-11).*

shown in figure 18.

## SKIN-FRICTION DRAG COEFFICIENT

The increase in the skin-friction drag coefficient resulting from the change in surface roughness was determined with the following relationships for incompressible conditions:

$$\Delta C_{D_f} = \frac{\Delta C_f A_w}{S}$$

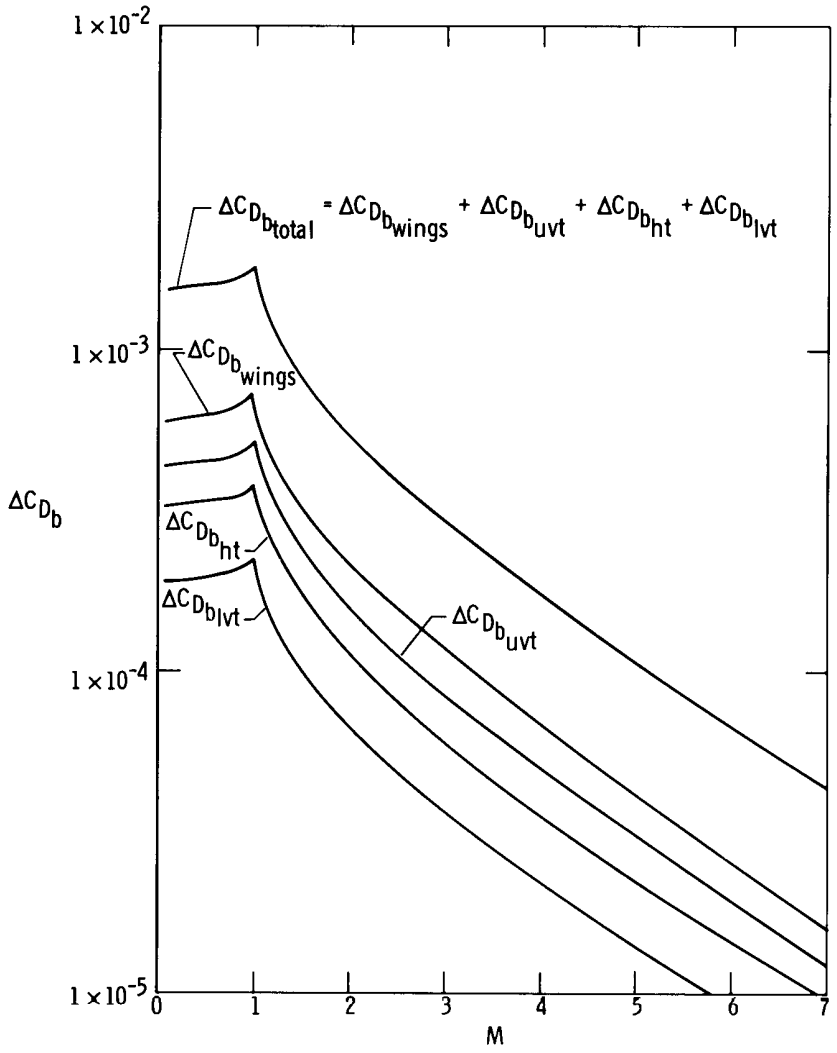


*Figure 18. Estimated increase in X-15-2 base drag coefficient caused by an applied ablative as a function of Mach number.*

with $\Delta C_f$ being obtained from the expression for turbulent flow

$$\Delta C_f = C_{f_{rough}} - C_{f_{smooth}}$$

where

$$C_{f_{rough}} = (1.89 + 1.62 \log l/k)^{-2.5} \quad \text{(ref. 13)}$$

and

$$C_{f_{smooth}} = \frac{0.455}{(\log R_l)^{2.58}} \quad \text{(ref. 13)}$$

The preceding relationships were applied for a family of roughness heights. (The clean airplane was assumed to be aerodynamically smooth.) The subscript $l$ represents the separate mean geometric chords for the wings, horizontal tails, upper vertical tail, modified fixed ventral fin, and fuselage. The results are shown in figure 19. To obtain the compressible skin-friction coefficients, figure 20 (fig. 12 of ref. 14) was used with the incompressible values of figure 19.

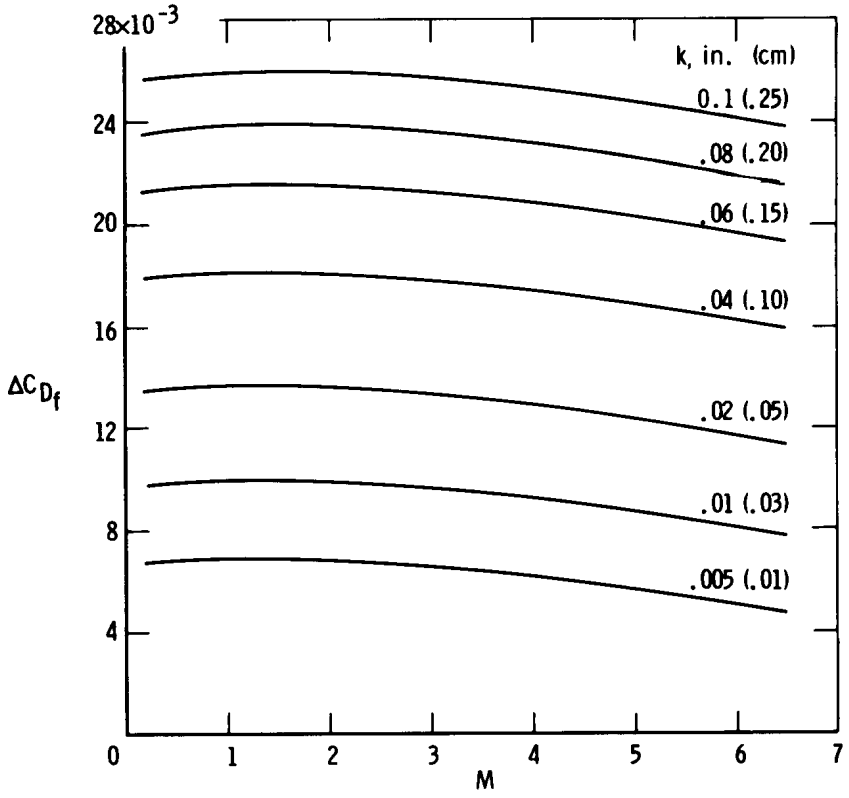


*Figure 19. Estimated incremental average skin-friction drag coefficient of the ablative coating as a function of Mach number for various roughness heights (based on incompressible data of ref. 13).*

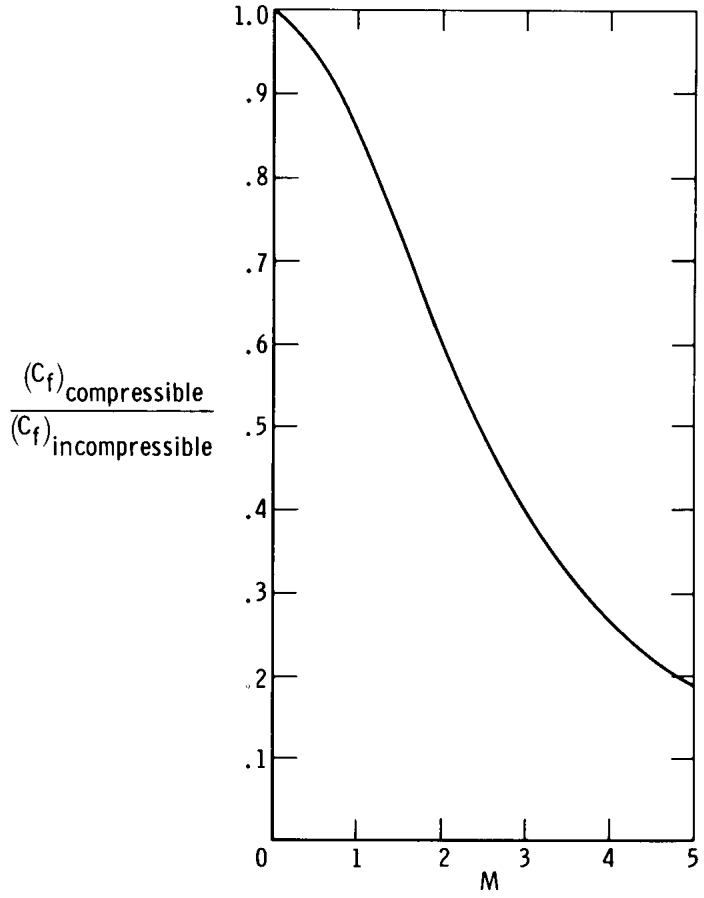


*Figure 20. Mach number variation of the ratio of the compressible to incompressible values of skin-friction coefficient for fully rough turbulent flow on an insulated plate (fig. 12 of ref. 14).*

## REFERENCES


1. Matranga, Gene J.: Analysis of X-15 Landing Approach and Flare Characteristics Determined From the First 30 Flights. NASA TN D-1057, 1961.

2. Saltzman, Edwin J.; and Garringer, Darwin J.: Summary of Full-Scale Lift and Drag Characteristics of the X-15 Airplane. NASA TN D-3343, 1966.

3. Rubert, Kennedy F.: Hypersonic Air-Breathing Propulsion-System Testing on the X-15. Progress of the X-15 Research Airplane Program, NASA SP-90, 1965, pp. 127-132.

4. Fisher, David F.: Flight-Measured Aerodynamic Drag of Two Large External Tanks Attached to the X-15-2 Airplane at Mach Numbers of 1.63 to 2.3. NASA TM X-1895, 1969.

5. Burcham, Frank W., Jr.; and Nugent, Jack: Local Flow Field Around a Pylon-Mounted Dummy Ramjet Engine on the X-15-2 Airplane for Mach Numbers From 2.0 to 6.7. NASA TN D-5638, 1970.

6. Cary, John P.: Experience With a Charring Ablator Heat Shield on the X-15-2 Airplane to Mach 6.7. NASA TM X-1745, 1969.

7. Beeler, De E.; Bellman, Donald R.; and Saltzman, Edwin J.: Flight Techniques for Determining Airplane Drag at High Mach Numbers. NACA TN 3821, 1956.

8. Wolowicz, Chester H.; and Gossett, Terrence D.: Operational and Performance Characteristics of the X-15 Spherical, Hypersonic Flow-Direction Sensor. NASA TN D-3070, 1965.

9. Larson, Terry J.; and Webb, Lannie D.: Calibrations and Comparisons of Pressure-Type Airspeed-Altitude Systems of the X-15 Airplane From Subsonic to High Supersonic Speeds. NASA TN D-1724, 1963.

10. Webb, Lannie D.: Characteristics and Use of X-15 Air-Data Sensors. NASA TN D-4597, 1968.

11. Watts, Joe D.: Flight Experience With Shock Impingement and Interference Heating on the X-15-2 Research Airplane. NASA TM X-1669, 1968.

12. Saltzman, Edwin J.: Base Pressure Coefficients Obtained From the X-15 Airplane for Mach Numbers up to 6. NASA TN D-2420, 1964.

13. Schlichting, Herman: Boundary Layer Theory. Pergamon Press, 1955.

14. Clutter, Darwin W.: Charts for Determining Skin-Friction Coefficients on Smooth and on Rough Flat Plates at Mach Numbers up to 5.0 With and Without Heat Transfer. Rep. No. ES 29074 (DDC No. AD 815 489), Douglas Aircraft Co., Inc., April 15, 1959.

15. Pyle, Jon S.; and Montoya, Lawrence C.: Effect of Roughness of Simulated Ablated Material on Low-Speed Performance Characteristics of a Lifting Body Vehicle. NASA TM X-1810, 1969.

16. Hoerner, Sighard F.: Fluid-Dynamic Drag. Publ. by the author (148 Busteed Dr., Midland Park, N. J.), 1965.

17. McLain, L. J.; and Palitz, Murray: Flow-Field Investigations on the X-15 Airplane and Model up to Hypersonic Speeds. NASA TN D-4813, 1968.

18. Penland, Jim A.: Aerodynamic Characteristics of a Circular Cylinder at Mach Number 6.86 and Angles of Attack up to 90°. NACA TN 3861, 1957.



NASA-Langley, 1970 —— 11 H-598